Tracing the journey of the sun and the solar siblings through the Milky Way

Martinez Barbosa, C.A.

Chapter 5

The effect of Galactic stellar encounters on the outer edge of the Solar System's parking zone

C.A. Martínez-Barbosa, L. Jílková, S. Portegies Zwart and A.G.A. Brown

Article in preparation.

Abstract

The frequency of Galactic stellar encounters the Solar System experienced depends on the local density and velocity dispersion at each position along the orbit of the Sun. The stronger encounters establish the outer limit of the so-called parking zone, which is the region in the plane of the orbital eccentricities and semi-major axes where the planetesimals of the solar system have been perturbed only by interactions with stars belonging to the Sun's birth cluster. We aim to improve the estimate of the number of encounters experienced

by the Sun in the past, as it serves to determine more accurately the outer edge of the parking zone. As a first step, we integrate the orbit of the Sun backwards in time in an analytical potential of the Milky Way. We use different present-day phase-space coordinates of the Sun, according to the measured uncertainties. The resulting orbits are then inserted in an N-body simulation of the Galaxy, where the stellar velocity dispersion is estimated at each position. We compute the Galactic stellar encounters by employing three different solar orbits. We found that the strongest stellar encounters have been with stars with $M = 0.1$ $M_\odot$ and at distances of $741 - 1320$ AU. These encounters set the outer edge of the Solar System's parking zone at semi-major axes of $300 - 1300$ AU, depending on the orbit of the Sun. These estimates are around one order of magnitude smaller than the determination made by Portegies Zwart & Jílková [2015].

keywords: planets and satellites: dynamical evolution and stability; Sun: general

5.1. Introduction

The Sun orbits in the gravitational potential of the Galaxy. The perturbations by passing stars [Oort, 1950] and by the Galactic gravitational field [Heisler & Tremaine, 1986] play an important role in the evolution of the most remote part of the Solar System, the so called Oort cloud. Oort [1950] suggested that more than 10^{11} icy bodies orbit the Sun with aphelia of 5–15 $\times$ 10^4 AU, and isotropically distributed inclinations of their orbital planes. The existence of the Oort cloud was proposed to explain the constant rate of observed new long period comets. The two mechanisms — the gravitational perturbation by the Galactic tide and the encounters with passing field stars — constantly perturb the Oort cloud sending some of its objects back into the planetary region. The Galactic tide has a stronger overall effect when averaged over long time scales [for example Heisler & Tremaine, 1986]. The effect of the encounters is stochastic and helps to keep the Oort cloud isotropic [e.g. Kaib et al., 2011,

and references therein]. The two mechanisms act together and combine in a non-linear way [Rickman et al., 2008].

It is well known that the disc of the Milky Way contains non-axisymmetric rotating patterns — the Galactic bar and spiral arms — which strongly influence the orbits of stars in the Galactic disc. For example, the stars can undergo so-called radial migration [for example Sellwood & Binney, 2002; Roškar et al., 2008a; Minchev & Famaey, 2010] which causes their orbital radii to change by up to several kiloparsec. It is possible that the Sun has experienced radial migration and spent a substantial time close to [Wielen et al., 1996; Minchev et al., 2013] or farther away from the Galactic centre compared to its present distance of about 8 kpc. However, some observational [e.g. Casagrande et al., 2011] and theoretical [e.g. Martínez-Barbosa et al., 2015] studies suggest that the Sun may not have migrated considerably.

The orbit of the Sun in the Galaxy determines the intensity of the gravitational tides the Solar System was exposed to, as well as the number of stars around the Sun that could pass close enough to perturb the Oort cloud. Kaib et al. [2011] investigated the effect of encounters with the field stars and the Galactic tides on the Oort cloud, considering the effect of the radial migration. They simulated the Oort cloud around the Sun, adopting possible solar orbits from the simulation of a Milky Way-like galaxy of Roškar et al. [2008a], including those that experienced no migration and those that experienced strong radial migration (some of their solar analogues get as close as 2 kpc from the Galactic centre and as far as 13 kpc, respectively). They found that the present day structure of the Oort Cloud depends rather strongly on the Sun's orbital history, in particular on its minimum past Galactocentric distance. The distance of the inner edge of the Oort cloud shows a similar dependence on the orbital history of the Sun and is in addition influenced by the effect of a few strong encounters between the Sun and other stars.

With the increasing amount of precise astrometric and radial velocity data for the stars in the solar neighborhood, several studies have focused on the identification of stars that passed close to the Solar System in the recent past, or will pass close by in the future [Mamajek et al., 2015; Bailer-Jones, 2015; Dybczyński & Berski, 2015]. For example, Mamajek et al. [2015] identified the star that is currently known to have made the closest approach to the Sun —

the so called Scholz's star that passed the Solar System at $0.25^{+0.11}_{-0.07}$ pc. Feng & Bailer-Jones [2015] studied the effect of recent and future stellar encounters, that is, those that are identified based on the observed positions and velocities of the stars in the solar neighborhood. They carried out simulations of the Oort cloud, considering perturbations by the identified encounters and a constant Galactic field at the current solar Galactocentric radius, and kept track of the flux of long-period comets injected into the inner Solar System as a consequence of the encounters. Unlike Kaib et al. [2011], Feng & Bailer-Jones [2015] focused only on the effect of the actually observed perturbers. They conclude that past encounters in their sample explain about 5% of the currently observed long period comets and they suggest that the Solar System experienced more strong, as yet unidentified, encounters.

Portegies Zwart & Jílková [2015] discuss the effect of the stellar encounter history on the structure of the system of planetesimals surrounding the Sun. They considered encounters with stars in the Sun's birth cluster (early on in the history of the Sun) and encounters with field stars that occur as the Sun orbits the Galaxy. The encounters with the field stars set the outer edge of the so called Parking zone of the Solar System [Portegies Zwart & Jílková, 2015]. The parking zone is defined as a region in the plane of semi-major axis and eccentricity of objects orbiting the Sun that have been perturbed by the parental star cluster but not by the planets or the Galactic perturbations. The orbits located in the parking zone maintain a record of the interaction of the Solar System with stars belonging to the Sun's birth cluster. Therefore, these orbits carry information that can constrain the natal environment of the Sun. Recently, Jílková et al. [2015] argued that a population of observed planetesimals with semi-major axes > 150 au and perihelia > 30 au, would live in the parking zone of the Solar System. They also found that such a population might have been captured from a debris disc of another star during a close flyby that happened in the Sun's birth cluster.

The outer edge of the parking zone is defined by the strongest encounter the Solar System experienced after it left its birth cluster. The strength of the encounter is measured by the perturbation of semi-major axes and eccentricity of the bodies in their orbit around the Sun. Portegies Zwart & Jílková [2015] used the impulse approximation [Rickman, 1976] to estimate the effect and

defined the outer edge of the Solar System's parking zone as corresponding to the perturbation caused by the Scholz's star [Mamajek et al., 2015]. However, stronger encounters might have happened in the past, as the Sun orbited in the Galactic disc. These encounters would alter the outer edge of the Solar System's parking zone moving it closer to the Sun. The perturbation strength of the stellar encounters depends on the characteristics of the close encounters with field stars — the mass of the other star, its closest approach and relative velocity. Similar to Scholz's star, the parameters of some of the recent close encounters can be derived from the observed data [for example Feng & Bailer-Jones, 2015; Dybczyński & Berski, 2015].

Estimates of the number and strength of past encounters are difficult to make because of the large uncertainties in the Galactic environment where the Sun has been moving since it left its birth cluster. These uncertainties are due to the unknown evolution of the Galactic potential (leading to uncertainties in the Sun's past orbit), which is in turn related to the unknown (population dependent) density and velocity dispersion of the Milky Way stars along the Sun's orbit. García-Sánchez et al. [2001] studied the recent encounter history of the Sun by integrating its orbit in an analytical Milky Way potential together with 595 stars from the Hipparcos catalogue in order to identify recent and near future encounters. In addition they estimated the encounter frequency for the Sun in its present environment by considering the velocity dispersions and number densities of different types of stars. Rickman et al. [2008] simulated the stellar encounters by assuming random encounter times (for a fixed number of encounters) over 5 billion years and using velocity dispersions for 13 different types of stars (different masses), with relative encounter frequencies for these types taken from García-Sánchez et al. [2001]. An alternative approach based on a numerical model of the Milky Way was taken by Kaib et al. [2011]. The orbits of solar analogues in this model were extracted from a simulation of a Milky Way-like galaxy and then the encounters were simulated by tracking the stellar number density and velocity dispersion along the orbit and then generating random encounters by starting stars at random orientations 1 pc from the Sun. The encounter velocities were generated using the recipe by Rickman et al. [2008].

In this chapter we set out to improve the estimate of the number of encounters the Sun may have experienced in the past, as this serves to better predict the location of the outer edge of the Solar System's parking zone. We compute the number of encounters by employing the largest Milky Way simulation to date, which contains 51 billion particles, divided over a central bulge, a disk and a dark matter halo [Bédorf et al., 2014]. This Galaxy model is used to estimate the velocity dispersion of the stars encountered by the Sun along its orbit. To achieve this we integrate the Sun's orbit back in time using an analytical potential for the Milky Way. The orbit of the Sun is then inserted in a snapshot of the particle simulation and the velocity dispersion of the disk stars is estimated at each position. We employ three different orbits for the Sun (no radial migration, migration inward, migration outward) and use the resulting estimates of the encounter frequencies as a function of stellar mass to discuss the implications for the location of the outer edge of the Solar System's parking zone.

This chapter is organized as follows: In Sect. 5.2 we explain the Galaxy model and we show three possible orbital histories of the Sun. In Sect. 5.3 we use the particle simulation of the Milky Way to estimate the number of encounters along each of these solar orbits, as a function of the mass and closest approach of the encountering star. In Sect. 5.4 we discuss the consequences of this computation on the estimation of the outer edge of the Solar System's parking zone. In Sect. 5.5 we discuss the limitations of our computation and the improvements that might be done in future studies. Finally in Sect. 5.6 we conclude.

5.2. Galaxy model and the solar orbit

We use an analytical potential to model the Milky Way to calculate potential past solar orbits. This Galactic potential is composed of two parts: an axisymmetric component (bulge, disk and dark matter halo) and a non-axisymmetric component (bar and spiral arms). Hereafter r and R represent the spherical and cylindrical radial coordinates respectively, φ is the azimuthal angle measured from the axis of the bar or spiral arms and in the direction opposite to the Galactic rotation, and z is the vertical component, perpendicular

Table 5.1: Modeling parameters of the Milky Way.

Axisymmetric component		
Mass of the bulge (M_b)	$1.41 \times 10^{10}\ M_\odot$	
Scale length bulge (b_1)	0.3873 kpc	
Disk mass (M_d)	$8.56 \times 10^{10}\ M_\odot$	
Scale length 1 disk (a_2)	5.31 kpc	1)
Scale length 2 disk (b_2)	0.25 kpc	
Halo mass (M_h)	$1.07 \times 10^{11}\ M_\odot$	
Scale length halo (a_3)	12 kpc	
Central Bar		
Pattern speed (Ω_bar)	55 km s^{-1} kpc^{-1}	2)
Mass (M_bar)	$9.8 \times 10^9\ M_\odot$	4)
Semi-major axis (a)	3.1 kpc	5)
Axis ratio (b/a)	0.37	5)
Vertical axis (c)	1 kpc	6)
Orientation	20°	3)
Spiral arms		
Pattern speed (Ω_sp)	25 km s^{-1} kpc^{-1}	2)
Number of spiral arms (m)	2	7)
Amplitude (A_sp)	$3.9 \times 10^7\ M_\odot$ kpc^{-3}	4)
Pitch angle (i)	15.5°	4)
Scale length (R_Σ)	2.6 kpc	7)
Scale height (H)	0.3 kpc	7)
Orientation	20°	5)

References: 1) Allen & Santillán [1991]; 2) Gerhard [2011]; 3) Romero-Gómez et al. [2011]; 4) Jílková et al. [2012]; 5) Martínez-Barbosa et al. [2015]; 6) Monari et al. [2014]; 7) Drimmel [2000]; 8) Jurić et al. [2008]

to the plane of the Galactic disk. In the computation of the solar orbit, r, R, φ and z are measured in a frame co-rotating with the bar. The force due to the spiral arms is therefore calculated by translating these coordinates to a frame co-rotating with the spiral arms.

In Sects. 5.2.1- 5.2.3 we give a detailed description of the axisymmetric and non-axisymmetric components of the Galactic potential.

5.2.1. Axisymmetric component

As mentioned before, the axisymmetric component of the Galaxy consists of a bulge, disk and a dark matter halo. We model the bulge of the Milky Way as a Plummer potential [Plummer, 1911]:

$$\Phi_{\rm bulge} = -\frac{GM_{\rm b}}{\sqrt{r^2 + b_1^2}}\,, \tag{5.1}$$

where G corresponds to the gravitational constant, $M_{\rm b}$ is the mass of the bulge, and b_1 is its corresponding scale length.

The disk of the Milky Way was modelled by using a Miyamoto-Nagai potential [Miyamoto & Nagai, 1975], which is described by the expression:

$$\Phi_{\rm disk} = -\frac{GM_{\rm d}}{\sqrt{R^2 + \left(a_2 + \sqrt{z^2 + b_2^2}\right)^2}}\,. \tag{5.2}$$

Here $M_{\rm d}$ corresponds to the mass of the disk. The parameters a_2 and b_2 are constants that modulate its shape. In particular, when $a_2 = 0$, Eq. 5.2 represents a spherical distribution of mass. In the case where $b_2 = 0$, Eq. 5.2 corresponds to the potential of a completely flattened disk.

Finally, we model the dark matter halo by means of a logarithmic potential of the form:

$$\begin{aligned}\Phi_{\rm halo} = &-\frac{GM(r)}{r} \\ &-\frac{GM_{\rm h}}{1.02a_3}\left[-\frac{1.02}{1+\Re^{1.02}} + \ln\left(1+\Re^{1.02}\right)\right]_r^{100}\,,\end{aligned} \tag{5.3}$$

where

$$M(r) = \frac{M_{\rm h}\mathfrak{R}^{2.02}}{1+\mathfrak{R}^{1.02}} \quad \text{and}$$
$$\mathfrak{R} = \frac{r}{a_3}\,.$$

In the expression of above, $M_{\rm h}$ represents the mass of the halo and a_3 its scale length.

The parameters in Eqs. 5.1, 5.2 and 5.3 were taken from Allen & Santillán [1991] and they are listed in Table 5.1. Although the model introduced by Allen & Santillán [1991] does not precisely represent the current estimates of the mass distribution in the Galaxy, this model has been widely used in studies of orbits of open clusters [Allen et al., 2006; Bellini et al., 2010] and in studies of moving groups in the solar neighbourhood [Antoja et al., 2009, 2011]. Moreover, Jílková et al. [2012] did not find substantial differences in the orbit of an open cluster when the axisymmetric component is described by a different more up-to-date model. Therefore, we do not expect that the modelling of the axisymmetric component of the Galaxy influences the results obtained in this study.

5.2.2. Galactic bar

We model the bar of the Galaxy with a three-dimensional Ferrers potential [Ferrers, 1877], which is represented by the following density

$$\rho_{\rm bar} = \begin{cases} \rho_0 \left(1-n^2\right)^k & n<1 \\ 0 & n \geq 1 \end{cases}\,. \tag{5.4}$$

Here $n^2 = {\rm x}^2/a^2 + {\rm y}^2/b^2 + {\rm z}^2/c^2$ determines the shape of the bar potential, where x, y and z correspond to coordinates measured in a frame corotating with the bar. The parameters a, b and c are the semi-major, semi-minor and vertical axes of the bar, respectively. ρ_0 represents the central density of the bar and k its concentration. Following Romero-Gómez et al. [2011], we chose $k = 1$.

The parameters that describe the bar such as its pattern speed, mass, orientation and axes are currently under debate [for a complete discussion see e.g. Martínez-Barbosa et al., 2015]. Hence, we used values that are within the ranges reported in the literature. These values are listed in Table 5.1.

5.2.3. Spiral arms

The spiral arms are usually represented as periodic perturbations of the axisymmetric potential. We use the prescription given by Cox & Gómez [2002], which models such perturbations in the three-dimensional space. The potential of the spiral arms is given by the following expression:

$$\begin{aligned}\Phi_{\rm sp} = &-4\pi G H A_{\rm sp} \exp\left(-\frac{r}{R_\Sigma}\right) \sum_n \left(\frac{C_n}{K_n D_n}\right) \times \\ &\cos(n\gamma) \left[\operatorname{sech}\left(\frac{K_n z}{\beta_n}\right)\right]^{\beta_n},\end{aligned} \tag{5.5}$$

where H is the scale height, $A_{\rm sp}$ is the amplitude of the spiral arms and R_Σ is the scale length. We use $n = 1$ term only, with $C_1 = 8/3\pi$ and the parameters K_1, D_1 and β_1 given by:

$$\begin{aligned}K_1 &= \frac{m}{r \sin i}, \\ \beta_1 &= K_1 H (1 + 0.4 K_1 H), \\ D_1 &= \frac{1 + K_1 H + 0.3 (K_1 H)^2}{1 + 0.3 K_1 H},\end{aligned}$$

where m and i correspond to the number of arms and pitch angle of the spiral structure respectively.

Finally, the term γ in Eq. 5.5 represents the shape of the spiral structure, which is described by the expression:

$$\gamma = m \left[\varphi - \frac{\ln(r/r_0)}{\tan i}\right].$$

Here r_0 is a parameter which determines the scale length of the spiral arms. Following Jílková et al. [2012], $r_0 = 5.6$ kpc.

As for the bar, the parameters that describe the spiral structure of the Galaxy are rather uncertain [See e.g. Jílková et al., 2012; Martínez-Barbosa et al., 2015]. Therefore, we chose the values that are consistent with the current picture of the spiral arms. These values are listed in table 5.1.

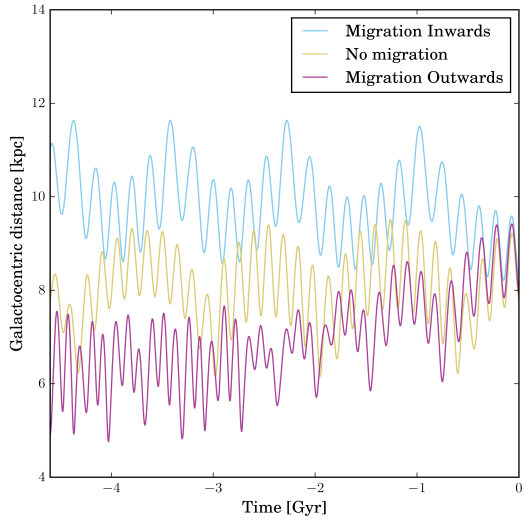

Figure 5.1: Possible trajectories of the Sun under the Galactic parameters listed in Table. 5.1. $t = 0$ Gyr represents the current time. The Galactocentric distance is measured in an inertial reference frame.

5.2.4. Solar orbits

We compute the orbit of the Sun backwards in time using the analytical Galaxy model described previously. In this calculation we account for the uncertainty in the present-day Galactocentric phase-space coordinates of the Sun. We employ the same methodology as used by Martínez-Barbosa et al. [2015] for this purpose[1]. Thus, we select a sample of 5000 random positions and velocities from a normal distribution centred at the current phase-space coordinates of the Sun. The normal distribution is then centred at $(r_\odot, v_\odot)$ with standard deviations (σ) corresponding to the uncertainties in these coordinates. The present day location of the Sun is:

$$r_\odot = (-8.5, 0, 0.02)\ \text{kpc} \quad \text{and}$$
$$\sigma_r = (0.5, 0, 0.005)\ \text{kpc}\,.$$

[1]Unlike Martínez-Barbosa et al. [2015] we use a three-dimensional model for the Galaxy in this study.

The present day velocity of the Sun is given by:

$$v_\odot = (11.1, 12.4 + V_{\rm LSR}, 7.25) \text{ km s}^{-1} \quad \text{and}$$
$$\sigma_v = (1.2, 2.1, 0.6) \text{ km s}^{-1}\,.$$

where $v_\odot$ and σ_v were taken from Schönrich et al. [2010] and $V_{\rm LSR}$ corresponds to the velocity in the Local Standard of Rest. According to the Milky Way model parameters listed in Table 5.1, $V_{\rm LSR} = 226$ km s^{-1}.

We integrate the orbit of the Sun backwards in time using each of the 5000 positions and velocities as initial phase-space coordinates. The solar orbits were computed during 4.6 Gyr by using a 6th-order integrator called Rotating Bridge [Martínez-Barbosa et al., 2015, Pelupessy et al. in prep.]. This integrator is implemented in the Amuse framework [Portegies Zwart et al., 2013; Pelupessy et al., 2013].

At the end of the simulation, we obtain a collection of solar orbits, from which we chose three. These orbits are shown in Fig. 5.1 and they represent different orbital histories of the Sun through the Galaxy. The blue orbit for instance shows that the Sun might have been born at $\sim$ 11 kpc from the Galactic centre, suggesting migration from outer regions of the Galactic disk to $R_\odot$. Martínez-Barbosa et al. [2015] argued that such a migration could only have happened if the Sun was influenced by the overlapping of the co-rotation resonance of the spiral arms with the Outer Lindblad resonance of the bar. Conversely, the violet orbit shows an example where the Sun migrated from inner parts of the disk to $R_\odot$, in accordance with Wielen et al. [1996] and Minchev et al. [2013]. The yellow orbit represents the case where the Sun does not migrate on average.

The stellar encounter rate experienced by the Sun during the last 4.6 Gyr depends on the solar orbit, due to differences in the stellar density and in the local stellar velocity dispersion. Therefore we compute the number of stellar encounters in each of the orbits shown in Fig. 5.1. The methodology is described in Sect. 5.3.

5.3. Galactic stellar encounters

The frequency of stellar passages between the Sun and other stars in the Galaxy is given by the following expression [i.e. Portegies Zwart & Jílková, 2015]:

$$\Gamma = n(t, x, y, z)\sigma(M, V, r_{\rm enc})\nu(x, y, z), \tag{5.6}$$

where x, y, z are the Galactocentric coordinates of the Sun at a given time t, measured in an inertial reference frame. M is the mass of the encountering star, V is its heliocentric velocity and $r_{\rm enc}$ is the closest approach distance of such a star to the Sun. The function $n(t, x, y, z)$ corresponds to the number of stars with mass M per unit volume, $\sigma(M, V, r_{\rm enc})$ is the gravitationally focused cross section and $\nu(x, y, z)$ is the local velocity dispersion. In the next paragraphs we describe the procedure to calculate these functions in detail.

The number of stars with mass M per volume is given by the expression: $n(t, x, y, z) = f\rho(t, x, y, z)$, where f is the fraction of stars with mass M and $\rho(t, x, y, z)$ is the local stellar density. f is calculated by the integration of an initial mass function (IMF) in a mass interval around M. We used a Kroupa IMF [Kroupa, 2001], with limiting masses between 0.08 and 100 $M_\odot$ to calculate f. In this mass range, the Kroupa IMF is described by the following expression:

$$\phi(m) = \begin{cases} \xi_1 m^{-1.3} & 0.08 < m \leq 0.5 M_\odot, \\ \xi_2 m^{-2.3} & m > 0.5 M_\odot. \end{cases} \tag{5.7}$$

Here ξ_1 and ξ_2 are normalization constants. For the mass range mentioned above, $\xi_1 = 1/4$ and $\xi_2 = 1/8$. The local stellar density on the other hand, is computed through the Poisson's equation using the Galaxy potential described in Sect. 5.2. In the calculation of the local stellar density, we do not include the dark matter halo potential.

The gravitationally focused cross-section in Eq. 5.6 can be computed from energy and angular momentum conservation laws. This quantity is thus given by the following expression [Binney & Tremaine, 1987]:

$$\sigma(M, V, r_{\rm enc}) = \pi r_{\rm enc}^2 \left(1 + \frac{2GM}{V^2 r_{\rm enc}}\right). \tag{5.8}$$

Here M and $r_{\rm enc}$ are independent free parameters, while V depends on the mass of the star. This heliocentric velocity is calculated by combining the peculiar velocity of the encountering star with the apex velocity of the Sun[2]. We refer the reader to Rickman et al. [2008] for further details on the calculation of V. In this study we use the final values of V listed in Rickman et al. [2008], Table 1.

Finally, we compute the velocity dispersion (ν) in all the regions of the Galaxy. We obtain ν by using the largest N-body simulation of the Milky Way, which employs a total number of 51 billion particles [Bédorf et al., 2014]. We did not use the Galactic model described in Sect. 5.2 given the complexity in the estimate of ν from an analytical Galaxy model. Although the computation of ν by means of a different Galaxy model is not consistent, we notice that the simulations of Bédorf et al. [2014] have successfully reproduced the stellar velocity distribution within 500 pc from the Sun (see e.g. Fig. 3 in their paper). For simplicity, we also do not take the temporal evolution of ν into account, that is, we calculate ν from a single snapshot. An approach in which the computation of $\rho(t, x, y, z)$ and $\nu(t, x, y, z)$ is made consistently is left for a future work.

We compute ν by using the snapshot of Bédorf's simulation corresponding to 5.6 Gyr of evolution. We chose this snapshot because it corresponds well to the current picture of the Milky Way. In this snapshot, we discretize the space in bins of $(\Delta_{\rm R}, \Delta_\varphi, \Delta_z) = (0.3 \text{ kpc}, 0.26 \text{ rad}, 5 \text{ pc})$ respectively. This choice ensures a robust estimate of ν because of the number of particles located at each bin. The region in the Galaxy where we determine ν is: $0 \leq R \leq 15$ kpc; $0 \leq \varphi \leq 2\pi$ rad and $-200 \leq z \leq 200$ pc.

The velocity dispersion is given by the following expression:

$$\nu^2 = \frac{\sum_{i=1}^{N} \left[(v_{{\rm R}_i} - \bar{v}_{\rm R})^2 + (v_{\varphi_i} - \bar{v}_\varphi)^2 + (v_{z_i} - \bar{v}_z)^2 \right]}{N - 1}, \tag{5.9}$$

where $v_{{\rm R}_i}, v_{\varphi_i}$ and v_{z_i} are the radial, tangential and vertical velocities of the i-th star in a bin of N stars. $\bar{v}_{\rm R}, \bar{v}_\varphi$ and $\bar{v}_z$ are the mean values of the former velocities respectively.

[2]These two vectors are measured in the local standard of rest of the encountering star.

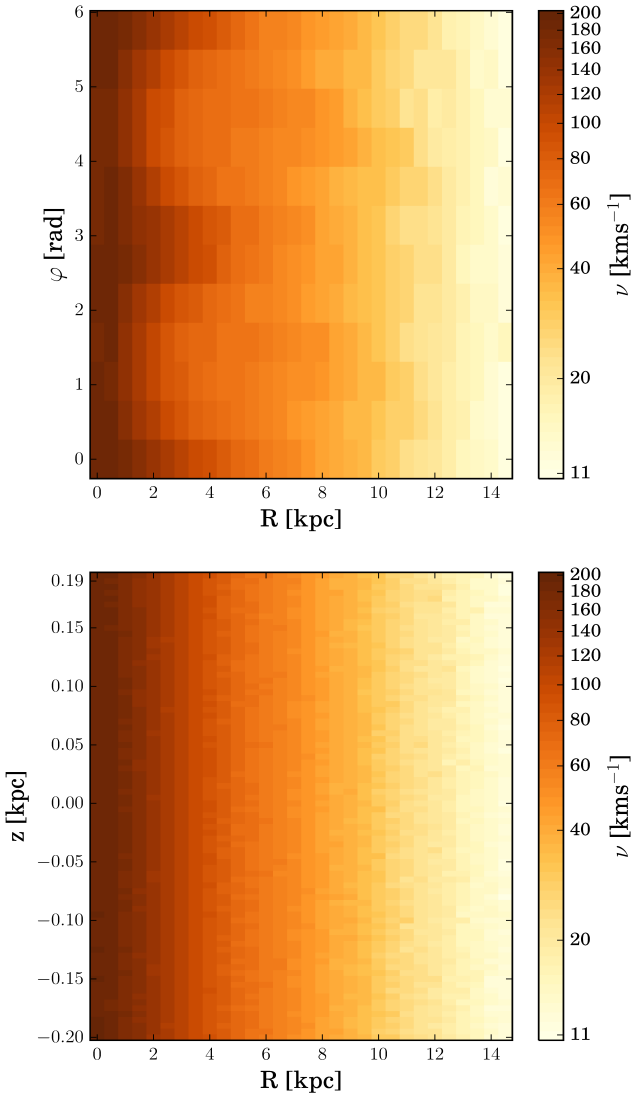

Figure 5.2: *T*op: Stellar velocity dispersion of the Milky Way as a function of Galactocentric radius and azimuth where $0 \leq z \leq 5$ pc. *B*ottom: Stellar velocity dispersion as a function of Galactocentric radius and vertical distance where $0 \leq \varphi \leq \pi/6$ rad.

In Fig. 5.2 we show ν as a function of the radius and azimuth (top panel) and as a function of the radius and vertical distance (bottom panel). As is expected, the velocity dispersion decreases with radius, due to a reduction of the stellar density in the outer regions of the Galaxy. At the solar position, we observe that $\nu \simeq 40$ km s^{-1}, which is in agreement with measurements of the local velocity dispersion [Nordström et al., 2004; Holmberg et al., 2009].

The velocity dispersion varies periodically with azimuth, being higher in the inner disk (e.g. top panel Fig. 5.2). This variation is a signature of the presence of the bar which extends up to ~ 4 kpc from the Galactic centre. The variation of ν with azimuth is smaller in outer regions of the disk and it is due to the presence of spiral arms. From Fig. 5.2 we also observe that the variation of the velocity dispersion with the vertical distance z is low compared to the change with radius or azimuth.

As we mention before, Eq. 5.6 gives the number of encounters between the Sun and another star in the Galaxy over a unit of time. The total number of encounters along the orbit of the Sun is thus given by:

$$n_{\rm enc} = \int_{t=0}^{4.6\ {\rm Gyr}} \Gamma(t, x, y, z, M, V, r_{\rm enc}) {\rm d}t. \tag{5.10}$$

In Fig. 5.3 we show contour lines of $n_{\rm enc}$ in terms of the mass and the closest distance of approach of the encountering star, for the three solar orbits shown in Fig. 5.1. The small bumps in the contours, specially when $n_{\rm enc} = 10^4$, are due to the binning in $r_{\rm enc}$, which is logarithmic and therefore, they are not related to some physical phenomenon. We analyze the number of encounters with stars that have a mass of $M = [0.1 - 5]\ M_\odot$, and the closest approach distance of $r_{\rm enc} = [10 - 10^6]$ AU (or $4 \times 10^{-5} - 5$ pc). As we can observe, the orbit moving closer to the Galactic centre (migration outwards) experiences more stellar encounters of a given mass and closest approach distance than the orbit that moves farther (migration inwards). This is expected, since the stellar density and the velocity dispersion are higher in regions closer to the Galactic centre.

From the large set of stellar encounters obtained, we can look for those that produce the strongest perturbation in the outer regions of the Solar System. These stellar encounters will set the outer edge of the parking zone. Portegies

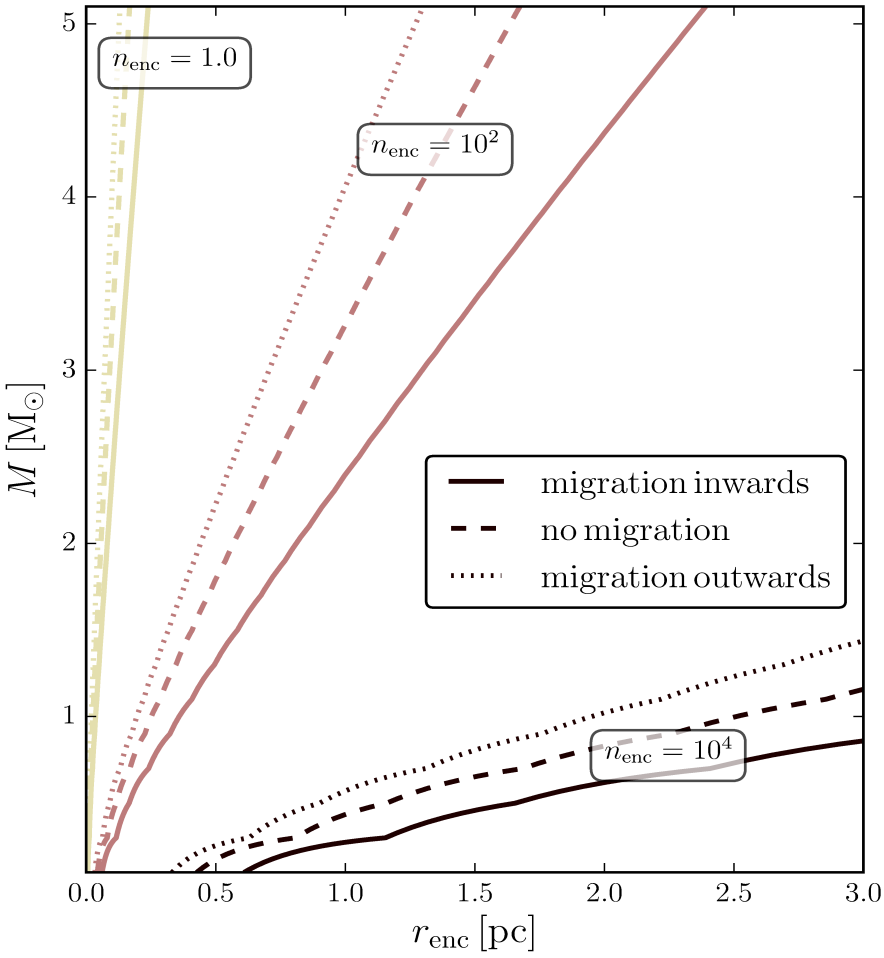

Figure 5.3: Contour lines of the Number of stellar encounters experienced by the Sun along its orbit (n_{enc}) in terms of the mass and the closest distance of the encountering star. The different line styles correspond to the solar orbits shown in Fig. 5.1.

Table 5.2: Stellar encounters that produce the strongest perturbation on objects orbiting the Sun. These encounters satisfy the condition $n_{\rm enc} \geq 1$.

Orbit	M [$M_\odot$]	$r_{\rm enc}$ [AU]	V [kms^{-1}]
Migration inwards	0.1	1320	5.1
No migration	0.1	932	5.1
Migration outwards	0.1	741	5.1

Zwart & Jílková [2015], used the encounter with Scholz's star to determine the location of the outer edge of the Solar System's parking zone. They found that the effect of this particular encounter has hardly perturbed the Oort cloud down to a distance of 10^5 AU. If the Sun experienced stronger stellar encounters (i.e. with closer and/or more massive stars), the perturbations in the Oort cloud might become important at smaller semi-major axes, shifting inwards the outer edge of the parking zone. In the next section we determine the strongest stellar encounters experienced by the Sun and we make a new estimate of the location of the outer edge of the Solar System's parking zone.

5.4. The outer limit of the parking zone

The outer edge of the parking zone is estimated for each of the studied orbits by considering the stellar encounters that have occurred at least once. That is, the stellar encounters that satisfy $n_{\rm enc} \geq 1$. From such encounters we determine — through the impulse approximation [Rickman, 1976] — the encounters that produce the strongest perturbation of the Solar system objects; that is, the perturbation for which the impulse gained is comparable to the velocity at aphelion, as calculated by Portegies Zwart & Jílková [2015].

In Table 5.2 we present the mass, distance of closest approach and relative velocity of the stellar encounters that produce the strongest perturbation of the Solar system for each studied orbit. Note that these encounters come from stars with $M = 0.1\,{\rm M}_\odot$, passing at distances comparable to the border between the inner and classical Oort cloud [$\sim$1500 AU, Trujillo & Sheppard, 2014]. These encounters are stronger than the one with Scholz's star, a binary system of 0.15 $\rm M_\odot$ that has recently encountered the Sun at a distance of

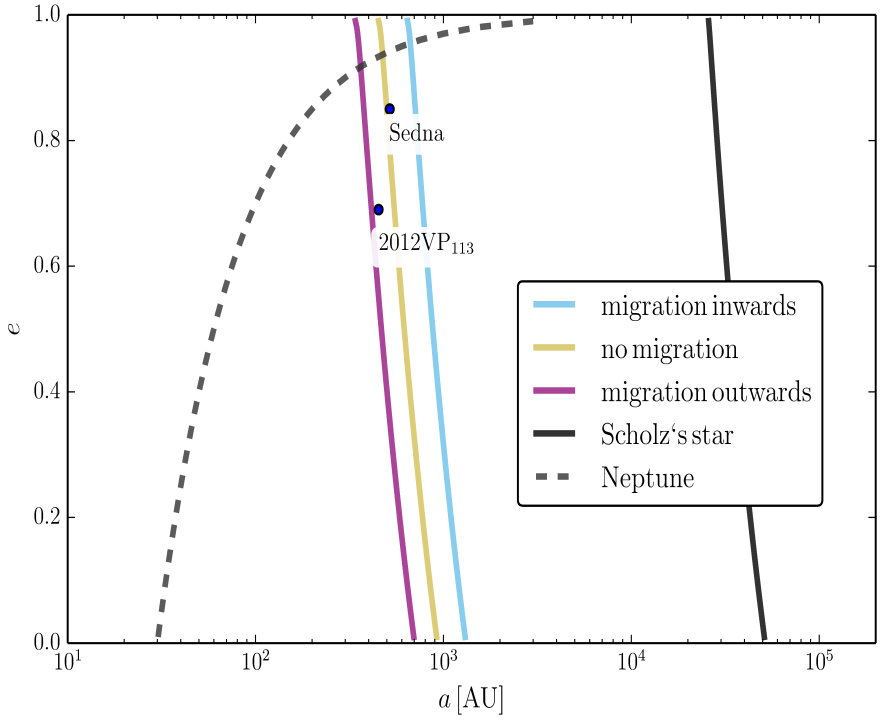

Figure 5.4: The penetration to which random Galactic stellar encounters affect the inner Solar System. e and a stand for eccentricity and semi-major axis respectively. The blue, yellow and purple lines show the outer edge of the Solar system's parking zone according to the solar orbits shown in Fig. 5.1. The black line is the estimate using Scholz's star [Portegies Zwart & Jílková, 2015]. The dashed black curve corresponds to the Neptune's perturbing distance, and indicates the inner edge of the parking zone. The two bullets give the orbital parameters for Sedna [Brown et al., 2004] and $2012VP_{113}$ [Trujillo & Sheppard, 2014].

$r_{\rm enc} = 0.25^{+0.11}_{-0.07}$ pc [or 50000 AU, Mamajek et al., 2015].

In Fig. 5.4 we show the outer edge of the Solar System's parking zone for the stellar encounters listed in Table 5.2. The solid black line corresponds to the previous estimate made by Portegies Zwart & Jílková [2015] using the Scholz's star. The outer edge of the parking zone given by the encounters derived here is located in the region corresponding to the inner Oort cloud, where objects like Sedna [Brown et al., 2004] and $2012VP_{113}$ [Trujillo & Sheppard, 2014] reside. The orbit migrating outwards from the denser inner regions of the Galaxy (violet line in Figs. 5.1 and 5.4), results in the smallest parking zone. The orbit migrating inwards from the less dense outer regions (blue line in Figs. 5.1 and 5.4) results in a parking zone that would not perturb the objects on Sedna-like orbits. This picture is consistent with Kaib et al. [2011], who concluded that the inner edge of the classical Oort cloud strongly depends on the orbit of the Sun, being smaller for the orbits that moved closer to the Galactic center.

5.5. discussion

We computed the Galactic stellar encounters in a more complete fashion than in Portegies Zwart & Jílková [2015]. However, we notice that our approach has some limitations. First, we use different Galaxy models to compute the local stellar density and the velocity dispersion along the orbit of the Sun. This is inconsistent, because the local density and the stellar velocity dispersion might be different in the two Galaxy models used, even when these models might reproduce the observed properties of the Milky Way locally. Second, since we used only one snapshot from the N-body Galaxy model, the velocity dispersion along the orbit of the Sun does not evolve with time.

We can improve the estimate of the stellar encounters by computing in a consistent manner the local stellar density and the velocity dispersion along the orbit of the Sun. This can be achieved by using either the analytical or the N-body Galaxy model. In the analytical Galaxy model, the velocity dispersion can be derived by solving the Jeans equations. In this way the temporal evolution of the velocity dispersion is also taken into account. However, several assumptions have to be made in order to obtain an uncomplicated solution for $\nu(t, x, y, z)$. For instance, it is necessary to assume an initial velocity dispersion profile and

the velocity ellipsoid aligned with the R and z axes. [Monari et al., 2013, Sect. 2.3]. In the analytical model of the Galaxy, the local stellar density is computed through the Poisson's equation, as explained in Sect. 5.3.

In the N-body Galaxy model on the other hand, it is necessary to integrate the orbit of the Sun and to compute $\rho(t, x, y, z)$ and $\nu(t, x, y, z)$ using this model to make a consistent determination of $n_{\rm enc}$. To account for the temporal evolution of ρ and ν, such calculations must include all the snapshots obtained from the N-body simulation. This procedure however, is not easy to execute given the complexity at handling the huge amount of data provided by each snapshot in the simulation.

The improvements mentioned above require further work and are outside the scope of this chapter. The computation of the encounter probability by using either of the two methods is left for a future work.

5.6. Summary and conclusions

We estimate the number of Galactic stellar encounters the Sun may have experienced in the past, along its orbit through the Galaxy. We aim to improve the previous estimates of the outer edge of the Solar System's parking zone made by Portegies Zwart & Jílková [2015]. The parking zone is the region in the plane of the eccentricity and semi-major axis where objects orbiting the Sun have been perturbed by stars belonging to the Sun's birth cluster but not by the planets or by Galactic perturbations. As a consequence, the orbits of objects located in the parking zone maintain a record of the interaction of the Solar System with the so called solar siblings [Portegies Zwart, 2009]. These orbits carry information that can constrain the natal environment of the Sun.

We use an analytical potential containing a bar and spiral arms to model the Galaxy. In this potential we integrate the orbit of the Sun back in time during 4.6 Gyr. Since we include the uncertainties in the present-day phase-space coordinates of the Sun, we obtain a collection of possible orbital histories. Here we study three different orbits, depending on the migration experienced by the Sun namely: migration inwards, no migration and migration outwards. The Galactic stellar encounters are estimated for each of these orbits.

We compute the number of Galactic stellar encounters by employing the

largest Milky Way simulation to date [Bédorf et al., 2014]. We insert the orbits of the Sun in a snapshot of this particle simulation and we estimate the velocity dispersion of the stars at each position. The resulting estimates of the encounter frequencies as a function of stellar mass and closest approach distance are used in the impulse approximation [Rickman, 1976] to determine the encounters that produce the strongest perturbation on the objects in the Oort cloud. Such stellar encounters determine the outer edge of the parking zone of the Solar System.

We found that the location of the outer edge of the parking zone depends on the solar orbit and that the Sun experienced stronger stellar encounters than those with the Scholz's star. As a consequence, the location of the outer edge of the parking zone is closer to the Sun than the previous estimates made by Portegies Zwart & Jílková [2015] and is comparable to the border between the inner and outer Oort cloud. Regardless of the migration of the solar orbit, we find that objects in the Solar System with semi-major axis smaller than 300 AU have not been perturbed by encounters with field stars. However, depending on the migration of the solar orbit, it is possible that the inner Oort cloud (including Sedna) has been perturbed.

To make a better estimate of the Galactic stellar encounters, it is necessary to evaluate the stellar density and the velocity dispersion at each position along the solar orbit using a Galaxy model that accounts for the evolution of the Milky Way. This would lead to a more refined determination of the outer edge of the parking zone.

Acknowledgements

This work was supported by the Nederlandse Onderzoekschool voor Astronomie (NOVA), the Netherlands Research Council NWO (grants #639.073.803 [VICI], #614.061.608 [AMUSE] and #612.071.305 [LGM]).